# Time-Resolved Fluorescence Anisotropy of HIV-1 Protease Inhibitor Complexes Correlates with Inhibitory Activity†

A. J. Kungl,*,‡ N. V. Visser,§ A. van Hoek,§ A. J. W. G. Visser,§ A. Billich,‡ A. Schilk,‡,|| H. Gstach,‡ and M. Auer*,‡

*Department of Immunology, Novartis Forschungsinstitut, Brunnerstrasse 59, A-1235 Wien, Austria, and Microspectroscopy Centre, Department of Biochemistry, Agricultural University, Dreyenlaan 3, 6703 HA Wageningen, The Netherlands*

*Received July 9, 1997; Revised Manuscript Received December 18, 1997*

ABSTRACT: The tryptophan time-resolved fluorescence intensity and anisotropy of the HIV-1 protease dimer is shown to be a quick and efficient method for the conformational characterization of protease inhibitor complexes. Four fluorescence lifetimes were needed to adequately describe the fluorescence decay of the two tryptophan residues, W6 and W42, per protease monomer. As a result of the wavelength dependence of the respective amplitudes, the 2.06 ns and the 4.46 ns decay constants were suggested to be the intrinsic fluorescence lifetimes of the more solvent-exposed W6 and the less exposed W42 residues, respectively. Analysis of the fluorescence anisotropy decay yielded a short correlation time of 250 ps corresponding to local chromophore motions, and a long correlation time of 12.96 ns resulting from overall rotation of the protease enzyme. Fluorescence lifetimes and rotational correlation times changed when inhibitors of the HIV-1 protease were added. The effects of 11 different inhibitors including statine-derived, hydroxyethylamine-derived, and 2 symmetrical inhibitors on the protease fluorescence dynamics were investigated. Inhibitor binding is shown to induce an increase of the mean fluorescence lifetime $\tau_{mean}$, an increase of the short rotational correlation time $\phi_1$, as well as a decrease of the long rotational correlation time $\phi_2$. The mean rotational correlation time $\phi_{mean}$ was identified as the global dynamic parameter for a given molecular complex, which correlates with the inhibitor dissociation constant $K_i$, and therefore with the activity of the inhibitor.

Human immunodeficiency virus (HIV)[1] is the causative agent for the acquired immunodeficiency syndrome (AIDS). Since the discovery of HIV, the search for agents that prevent the spread of this retrovirus has become a major research activity. For this purpose, a number of targets for chemotherapy have been identified based on the life cycle of the virus (*1*, *2*). One of the best investigated among these targets is the HIV-1 protease (*3*). Recently, a very successful combination treatment of AIDS by nucleoside-derived antiretroviral agents, which target reverse transcriptase, and saquinavir (*Invirase*, Roche), a protease inhibitor, has gained much scientific and public interest (*4*).

The HIV-1 protease is a homodimeric aspartyl protease which contains 99 residues per monomer. The specific task of this enzyme is to proteolytically cleave two precursor polypeptides which are initially translated from the *gag* and the *pol* viral genes. The results of this processing are structural proteins and enzymes, among them the protease itself, which are essential for the life cycle of the virus. Efficient digestion of the precursor is controlled by the specificity of the protease for certain amino acids at the cleavage site and for certain conformations of the polypeptide substrate. The active site of the HIV-1 protease can accommodate six to eight amino acids and consists of two aspartic residues at positions 25 and 25′ and the flexible glycine-rich $\beta$ strands or "flaps" (one from each monomer) (*5*). The first X-ray structure of the HIV-1 protease was solved by Wlodawer et al. (*6*). Since then, a wealth of three-dimensional data has been published, including many structures of the protease in complex with inhibitors (for review, see ref *7* and *8*). The binding cleft of the HIV-1 protease is formed at the interface between the identical monomeric subunits (Figure 1). One essential requirement for catalytic activity is a water molecule which is hydrogen bonded between the backbone amide hydrogens of the two isoleucine residues at positions 50 and 50′. In peptide-based inhibitor complexes, this water molecule donates two hydrogen bonds to carbonyl oxygens of the bound inhibitor, thereby inducing the fit of the flaps over the inhibitor (*9*).

Characteristically, aspartyl proteases are inhibited by the naturally occurring pentapeptide pepstatin A isolated from *Streptomyces* (*10*). Therefore, initial strategies for protease

† This work was supported by the Austrian Academy of Sciences (APART Fellowship Nr. 246 to A.J.K.).

* To whom correspondence should be addressed at the Department of Immunology, Novartis Forschungsinstitut, Brunnerstrasse 59, A-1235 Vienna, Austria. Telephone: +43 1 86634 257/259. FAX: +43 1 86634 582. E-mail: manfred.auer@pharma.novartis.com or andreas.kungl@pharma.novartis.com.

‡ Novartis Forschungsinstitut.

§ Agricultural University.

|| Present address: Boehringer Ingelheim R&D Vienna, Bender & Co., Dr. Boehringergasse 5-11, A1121 Vienna, Austria.

[1] Abbreviations: HIV, human immunodeficiency virus; AIDS, acquired immunodeficiency syndrome; MEM, maximum entropy method.

S0006-2960(97)01654-1 CCC: $15.00 
Published on Web 02/13/1998

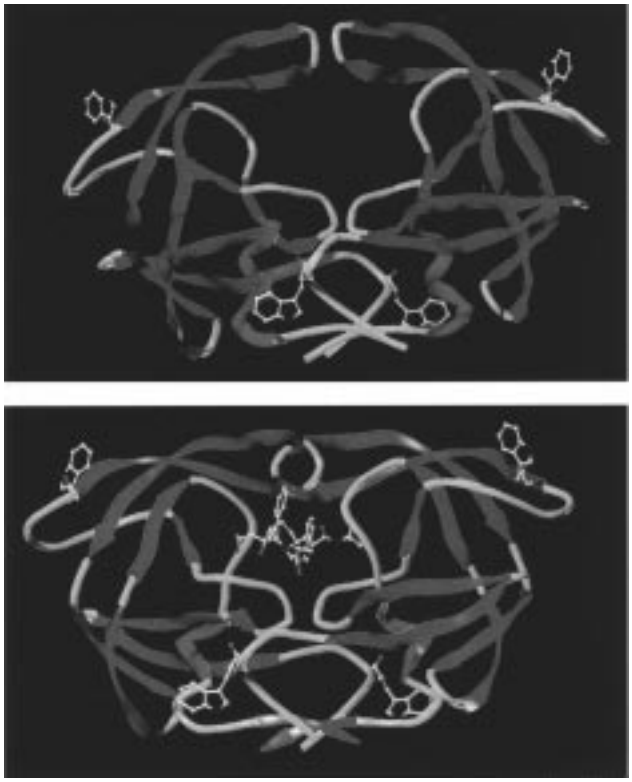

FIGURE 1: Ribbon-tube drawing of the X-ray structures of (A, top) the HIV-1 protease and (B, bottom) the complex of the protease with **6** (*Invirase*). The coordinates were taken from the Brookhaven data bank, entries 3phv (HIV-1 protease) and 1hxb (*Invirase* complex). The structures have been displayed with the program SYBYL 6.3 (TRIPOS Inc.) showing α helixes as red ribbons, $\beta$ sheets as blue arrows, and turns as yellow tubes. The tryptophan residues and the *Invirase* structure are shown in a ball-and-stick representation.

inhibitors focused on peptide analogues containing statine as the transition state analogue. At present, the majority of protease inhibitors are based on isosteric replacements for the dipeptide at the scissile bond of the substrate. The most potent isosteres are hydroxymethylene, hydroxyethylene, and hydroxyethylamine derivatives with inhibition constants ($K_i$) in the low nanomolar range (*11*). Recently, inhibitors containing the aminobenzylstatine moiety as the transition state analogue were shown to be antivirally active with a high oral bioavailability (*12*). Alternatively, modified natural substrates with transition state mimics or nonhydrolyzable analogues of specific amino acids at the cleavage site were demonstrated to be efficient protease inhibitors (*13*). More novel approaches to the identification of inhibitors include symmetry considerations (*14, 15*) as well as computerized searches of three-dimensional databases (*16*).

Fluorescence intensity and anisotropy decays of protein-intrinsic tryptophan and tyrosine residues are valuable tools for studying protein conformations and their molecular dynamics (*17*). Local motions, such as side chain and backbone fluctuations, occur on a pico- and nanosecond time scale which can be monitored using time-resolved fluorescence spectroscopy. These motions can therefore influence the transient emission profiles of intrinsic chromophores if there is a basic photophysical interaction mode. This may be quenching of the fluorescence by a variety of mechanisms such as excited-state collisions, electron or proton transfer, and also the radiationless transfer of electronic excitation energy (*18*). In addition, the fluorescence anisotropy decay is the result of the fluorophore dynamics and the overall rotation of the macromolecule (*19*). Structural and dynamic details of the chromophore(s) and its environment are therefore reflected in the fluorescence intensity and anisotropy decays. A thorough analysis of both becomes possible if the three-dimensional structure of the protein is known (*20*−*22*). Therefore, the two tryptophan residues per HIV-1 protease monomer, W6/W6′ and W42/W42′ (see Figure 1), were used as sensors in the present study to investigate the local and global structural dynamics of the protease with further emphasis on conformational and dynamic changes upon binding of high-affinity statine, hydroxyethylamine, and symmetrical inhibitors.

## MATERIALS AND METHODS

*Purification of HIV-1 Protease*. HIV-1 protease was expressed in *E. coli* (strain JM 105) using the expression plasmid pTZprt$^+$ (*23*). The enzyme was then purified to homogeneity as described in detail previously (*24*). The activity of the protease was checked immediately before measurements according to Richards et al. (*25*).

*Synthesis of Inhibitors*. Synthesis and testing of antiviral activity of the statine-derived inhibitors **1**−**5** have been described previously (*12, 26*−*28*). Also the synthesis of the more novel paracyclophane-containing statine-derived protease inhibitors, **7** and **8**, has been reported recently (*29*). The synthesis of *Invirase* Ro 31-8959 **(6)** as well as of **9** and the two symmetric inhibitors **10** und **11** followed published protocols (*15, 30*−*32*).

For the time-resolved fluorescence measurements, a freshly prepared 1 $\mu$M protease solution was prepared in 100 mM NaOAc (pH 4.7) and 1 M NaCl. This enzyme concentration resulted in a sufficient fluorescence intensity signal and was still low enough to avoid unspecific aggregation. All fluorescence measurements were recorded at 37 °C and were background-corrected for buffer (+inhibitor) autofluorescence. The buffer conditions were chosen according to conditions of the HIV-1 protease's maximum biological activity. For the measurements of protease inhibitor complexes, the inhibitors were added in a 10-fold molar excess, yielding at least 95% complex formation.

*The inhibitor dissociation constants, $K_i$ values,* were calculated from the inhibitors' $IC_{50}$ values according to *(48)* $IC_{50} = E_t/2 + K_i(1 + S/K_m)$, where $E_t$ is the total enzyme concentration, $S$ is the substrate concentration, and $K_m$ is the Michaelis constant for the substrate. The $IC_{50}$ values of the inhibitors were obtained by fitting the initial velocity data ($V$) from the inhibition of substrate hydrolysis to $V = V_0(IC_{50})/(I + IC_{50})$ where $I$ denotes the inhibitor concentration and $V_0$ is the velocity of the uninhibited reaction.

*Steady-state fluorescence spectra* were recorded on a SLM 8000C fluorometer (SLM Instruments, Urbana, IL). Fluorescence excitation spectra were corrected for the wavelength characteristics of the xenon lamp by the ratio mode method, and fluorescence emission spectra were corrected for buffer background emission. Commonly, slit widths giving a bandwidth of 2 nm were used. The integration time for 1 nm steps was 1 s in a 1 cm path length cuvette. All fluorescence measurements were performed with polarizers in the magic angle setting to reduce the influence of stray light.

Table 1: Parameters of MEM Fluorescence Decay Analysis

| substance | $A_1$ (%) | $\tau_1$ (ps) | $A_2$ (%) | $\tau_2$ (ps) | $A_3$ (%) | $\tau_3$ (ns) | $A_4$ (%) | $\tau_4$ (ns) | $\tau_{mean}$ (ns) | $\chi^2$ |
|---|---|---|---|---|---|---|---|---|---|---|
| apo | 1.7 | 204 | 26.0 | 444 | 45.6 | 2.06 | 26.5 | 4.46 | 2.23 | 1.13 |
| **1** | − | − | 26.0 | 468 | 46.5 | 2.08 | 27.3 | 4.61 | 2.34 | 1.20 |
| **2** | − | − | 25.4 | 558 | 49.5 | 2.27 | 24.9 | 4.90 | 2.48 | 1.50 |
| **3** | 23.8 | 422 | 45.0 | 2090 | 19.0 | 3.69 | 12.0 | 5.49 | 2.40 | 1.30 |
| **4** | − | − | 25.4 | 454 | 49.3 | 2.16 | 25.1 | 4.75 | 2.37 | 1.27 |
| **5** | − | − | 25.6 | 461 | 42.1 | 2.03 | 32.2 | 4.31 | 2.36 | 1.20 |
| **6**[a] | − | − | 24.0 | 505 | 50.3 | 2.10 | 25.5 | 4.17 | 2.23 | 1.36 |
| **7** | − | − | 25.2 | 489 | 49.7 | 2.20 | 24.9 | 4.79 | 2.40 | 1.38 |
| **8** | − | − | 23.9 | 436 | 48.6 | 2.07 | 27.3 | 4.65 | 2.37 | 1.27 |
| **9** | 7.3 | 214 | 20.2 | 475 | 44.2 | 2.05 | 28.0 | 4.47 | 2.26 | 1.17 |
| **10** | − | − | 26.6 | 491 | 49.8 | 2.24 | 23.5 | 4.87 | 2.37 | 1.25 |
| **11** | − | − | 25.0 | 485 | 48.9 | 2.24 | 25.9 | 5.02 | 2.51 | 1.31 |

[a] *Invirase* (Roche).

*Time-resolved fluorescence and anisotropy spectra* were recorded according to the single-photon counting method (*33*), as described previously (*34*, *35*). In short, the frequency-doubled output of a DCM dye laser, which was synchronously pumped by a mode-locked Nd:YLF laser (Coherent, Palo Alto, CA), was used as excitation source at 300 nm. The emission was collected through a combination of a WG320 cutoff filter and narrow band interference filters (all from Schott, Mainz, Germany): 321.4, 329.9, 348.8, and 374.6 nm. The resulting fluorescence decays were background-corrected by subtracting the fluorescence decay of the buffer (plus inhibitor) solution recorded under the same conditions as the protease (plus inhibitor) decay. The instrument response function was determined by measuring the ultrafast fluorescence decay of *p*-terphenyl ($\tau = 25$ ps) in a solution of cyclohexane/$CCl_4$ (1:1, v/v) (*36*).

*Time-resolved data analysis* was performed using the commercially available maximum entropy program MEMSYS5 (MEM, Maximum Entropy Solutions, Ely, U.K.), the principle of which has been extensively described in the literature (*37*, *38*). For the analysis of the fluorescence decay, a distribution of 150 equally spaced lifetime values $\tau$ on a log($\tau$) scale between 0.01 and 20 ns with amplitudes $\alpha$ were used. The same was done for the analysis of the fluorescence anisotropy decay: 150 equally spaced rotational correlation time values, $\phi$, on a log($\phi$) scale from 0.05 to 100 ns were used. The starting distribution models were chosen to be flat since no a priori knowledge about the system was available. In all cases, the $\chi^2$ values were close to 1.0 (see Table 1), and the weighted residuals as well as the autocorrelation of the residuals were randomly distributed around zero indicating an optimal fit.

## RESULTS

*Steady-State Fluorescence.* The fluorescence emission spectrum of the HIV-1 protease is typical for a tryptophan-containing protein in aqueous solution (*39*) with maximum intensity at 341 nm (see Figure 3). The small blue shift compared to the emission maximum of tryptophan in water [$\lambda_{em}$(max) = 348 nm] refers to chromophores shielded from the solvent. The position of the peak was found to depend on the excitation wavelength, shifting from 341 to 344 nm when excited at 275 and 305 nm, respectively. This shift is the result of selectively exciting the two tryptophan fluorophores W6 and W42 which are located in different environments (Figure 1) and therefore emit at different wavelengths (*18*). Also shown in Figure 3 is the fluorescence excitation spectrum of the protease which was recorded at an emission wavelength of 346 nm and yielded maximum intensity at 284 nm.

*Time-Resolved Fluorescence Intensity Decay.* A typical time-resolved fluorescence decay of the protease is shown in Figure 4 together with the respective data analysis by the maximum entropy method (MEM). The decay was recorded at 310 K with the excitation wavelength set at 300 nm, and the emission was collected at 348 nm. The transient was found to be highly nonexponential, being best fitted by four fluorescence lifetime centers (Figure 4B) giving a mean lifetime $\tau_{mean} = 2.23$ ns (see Table 1). The subnanosecond lifetimes $\tau_1 = 0.20$ ns and $\tau_2 = 0.44$ ns are interpreted as the result of excited-state quenching of the tryptophan emission by the protein backbone (*40*). The lifetimes $\tau_3 = 2.06$ ns and $\tau_4 = 4.46$ ns are typical decay times for the tryptophan's indole moiety in environments of different polarity.

The fluorescence of tryptophan itself is reported to decay biexponentially in aqueous solutions with decay times $\tau_1 = 0.5$ ns and $\tau_2 = 3.1$ ns corresponding to different side chain rotamer conformations (*41*). In the case of the HIV-1 protease fluorescence, it seemed therefore reasonable to assume that the four fluorescence lifetimes arise from the independently emitting tryptophan species W6 and W42. In order to obtain a model of the individual tryptophan-associated decays, total fluorescence intensity decays of the protease were recorded at different emission wavelengths. The emission wavelength was selected by inserting cutoff filters in the emission path instead of a monochromator, because the aim of the experiments was to collect maximum data quality within a minimum of time.

Reducing the emission wavelength from 348 to 321 nm resulted in a significant increase of the ratio between the picosecond fluorescence lifetime amplitude areas $A_1/A_2$ from 0.06 to 0.40. In contrast to the amplitude ratio of the picosecond lifetimes, the amplitude ratio of the nanosecond lifetimes $A_4/A_3$ remained constant. On increasing the emission wavelength to 374 nm, the amplitude area $A_1$ disappeared completely, and the ratio $A_4/A_3$ was reduced from 0.58 (at 348 nm) to 0.46. From this pairwise wavelength dependence of the protease fluorescence amplitude areas, and assuming independently emitting chromophores, two lifetime pairs were tentatively identified. $A_1(\tau_1)$ and $A_4(\tau_4)$ both decrease with increasing wavelength and were therefore

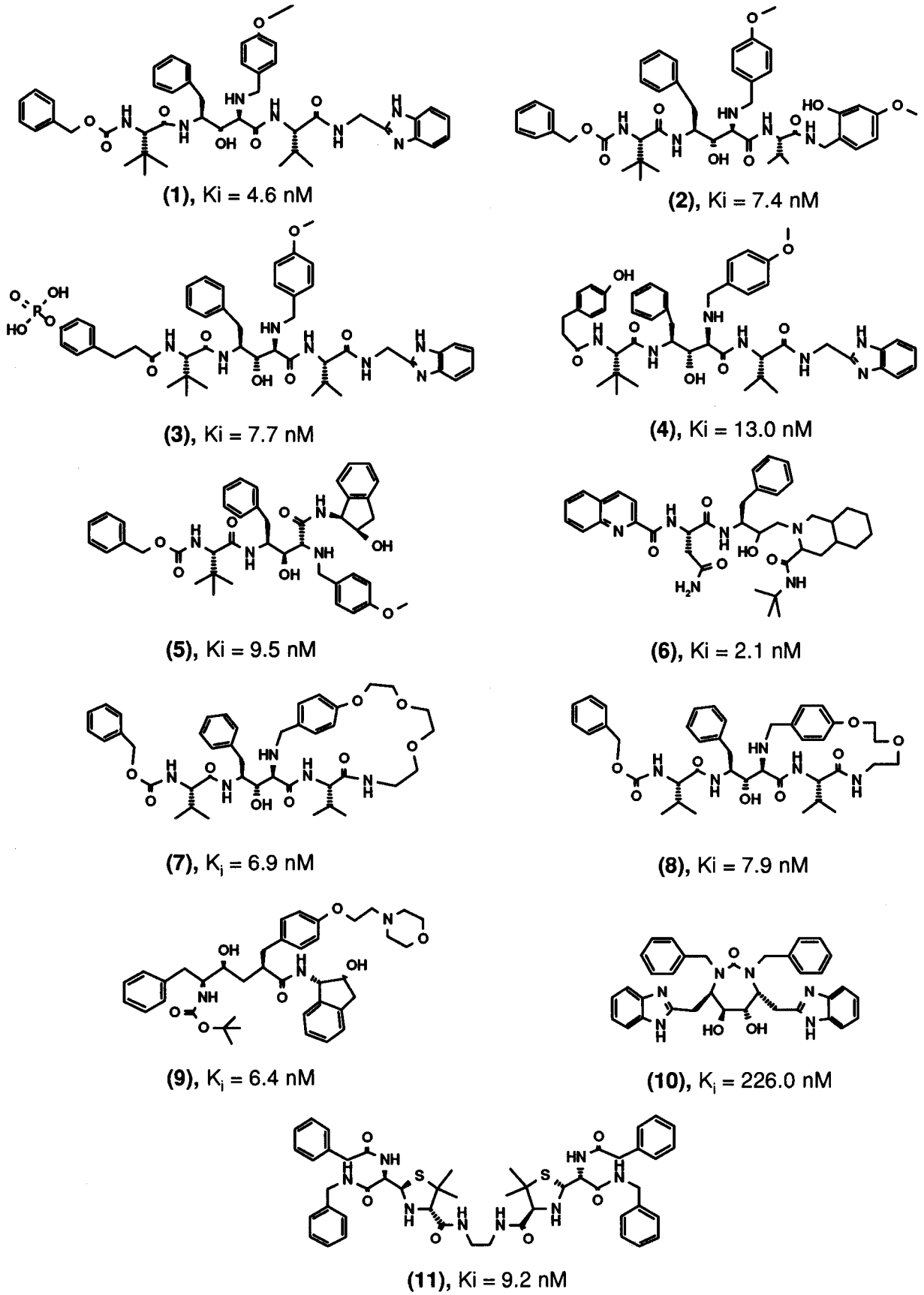


FIGURE 2: Structures of HIV-1 protease inhibitors. The $K_i$ values (in nanomolar) are shown. The trade name of substance **6** is *Invirase* (Roche).

associated to the blue-emitting tryptophan chromophores. On the other hand, $A_2(\tau_2)$ and $A_3(\tau_3)$ both increase with increasing wavelength and were therefore associated to the red-emitting tryptophan chromophores. A red shift of the tryptophan fluorescence is commonly associated with solvent-exposed residues, whereas a blue shift is associated with

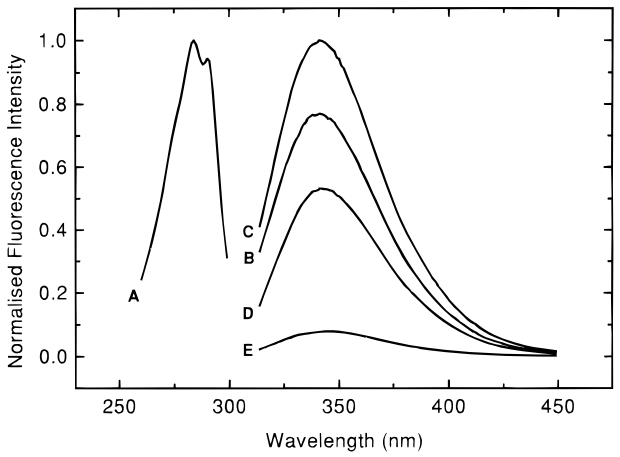


FIGURE 3: Steady-state fluorescence excitation and emission spectra of 1 $\mu$M HIV-1 protease in 100 mM NaOAc (pH 4.7), 1 M NaCl, at 37 °C (curves A and B−E, respectively). Curve A was recorded with an emission wavelength of 346 nm. Curves B−E were recorded with excitation wavelengths of 275, 285, 295, and 305 nm, respectively.

chromophores situated in a more hydrophobic environment (*42*). The W6 chromophores are located on a turn close to the protease core region (see Figure 1) and are more exposed to solvent than the W42 chromophores, which are located in a $\beta$ sheet within the flap regions. We therefore suggest that $\tau_2$ and $\tau_3$ are the intrinsic lifetimes of the W6 chromophores and $\tau_1$ and $\tau_4$ are the intrinsic lifetimes of the W42 chromophores.

Furthermore, this interpretation was supported by our recent molecular dynamics (MD) computer simulations of the HIV-1 protease. These numerical studies were mainly undertaken to calculate the theoretical anisotropy of the enzyme itself as well as in complex with inhibitors, from the tryptophan's MD trajectories (Ringhofer et al., manuscript in preparation). For this purpose, it was a major prerequisite to account for the relative contributions of the tryptophan species, W6/W6′ and W42/W42′, to the fluorescence decay. The best agreement of the calculated anisotropy decay with the experimental anisotropy decay was obtained if we took the ratio 2:1 for the contribution of W6 over W42. This is identical to the ratio of the amplitude area ratios $A_3$ relative to $A_4$, which represents, according to our interpretation of the wavelength-dependent fluorescence intensity decays, the weights of the W6 and W42 intrinsic lifetimes $\tau_3$ and $\tau_4$, respectively.

*Time-Resolved Fluorescence Anisotropy Decay.* The fluorescence anisotropy decay of HIV-1 protease at 310 K is shown in Figure 5A. MEM analysis revealed two narrow rotational correlation time distributions at $\phi_1 = 0.25$ ns and at $\phi_2 = 12.96$ ns with relative amplitudes $B_1 = 19.2\%$ and $B_2 = 80.8\%$, respectively. It is commonly assumed that the fluorescence of proteins is depolarized (i) by rapid local motions of the tryptophan side chain(s) and (ii) by the overall rotation of the entire macromolecule (*19*). In the case of HIV protease, this means that both the W6 and the W42 side chains move very rapidly according to their few hydrophobic contacts, which is reflected in the small value of $\phi_1$. The overall rotation is related to the hydrodynamic volume $V$ by the Einstein−Stoke's equation $\phi_2 = \eta V/RT$ ($\eta$ is the viscosity of the medium at the temperature $T$, and $R$ is the gas constant). The calculated hydrodynamic volume of the HIV-1 protease equals $8.02 \times 10^4$ Å$^3$, which corresponds to a molecular radius $r = 26.7$ Å. From the crystal structure (*6*), it is well-known that the protease molecule is disk-shaped (Figure 1) displaying a maximum diameter of ∼52 Å. The hydrodynamic radius computed from the long rotational correlation time $\phi_2$ therefore agrees very well with the 3-D structure of the HIV-1 protease.

At 323 K, the anisotropy of the protease does not decay to zero but instead reaches a plateau at the limiting anisotropy value of 0.07 (data not shown). Unspecific aggregation at higher temperature is the reason for this limiting anisotropy which, however, did not lead to precipitation of the enzyme. At 283 K, on the other hand, both rotational correlation times $\phi_1$ and $\phi_2$ increased compared to 310 K. The increase is the result of a general decrease in both local and overall motion at lower temperatures.

*Time-Resolved Fluorescence of HIV-1 Protease Inhibitor Complexes.* The effect of 11 potent inhibitors (see Figure 2) of the HIV-1 protease on the fluorescence and anisotropy decay of the enzyme was investigated. The results obtained

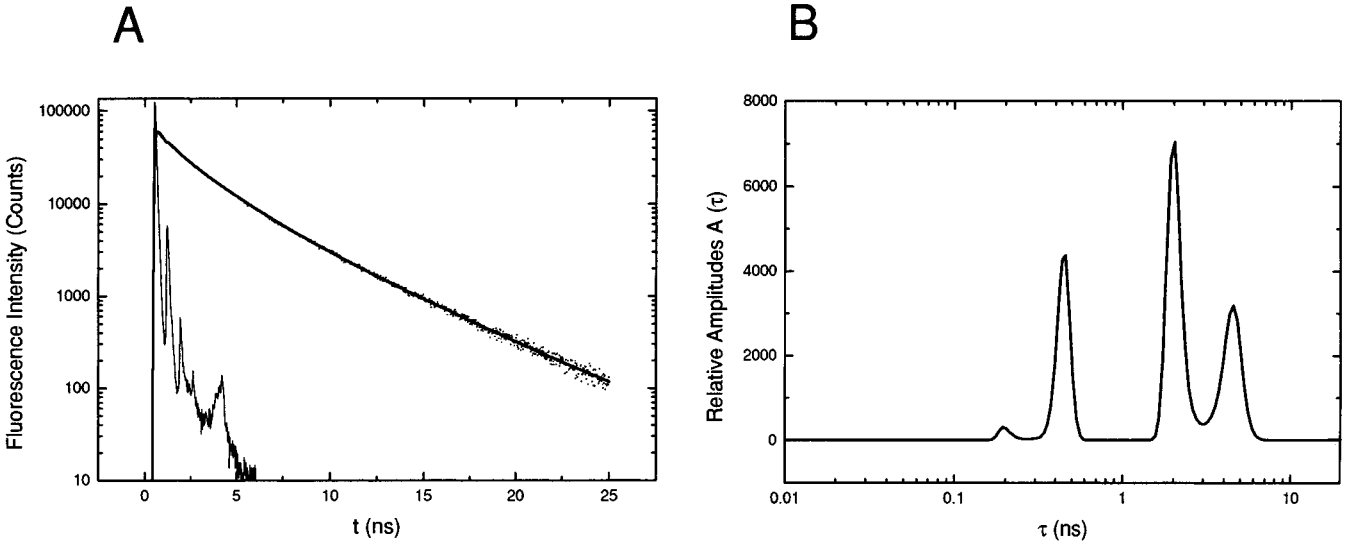


FIGURE 4: Time-resolved fluorescence intensity decay (A) and MEM analysis (B) of 1 $\mu$M HIV-1 protease in 100 mM NaOAc (pH 4.7), 1 M NaCl, at 37 °C. Excitation was set at 300 nm, and emission was collected at 348.8 nm.

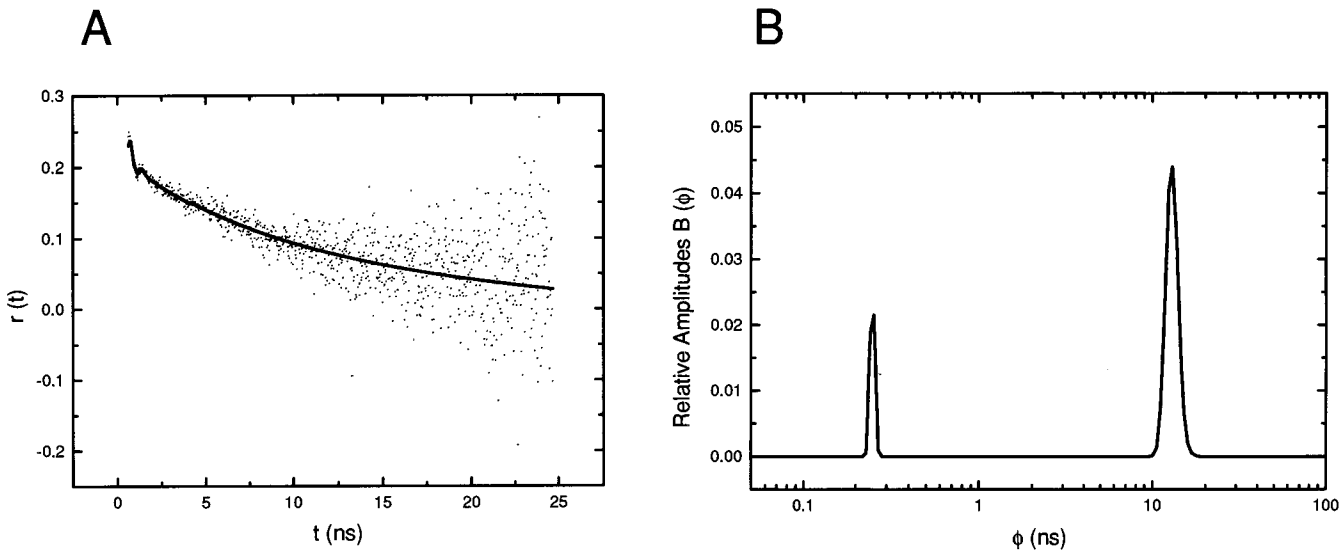


FIGURE 5: Time-resolved fluorescence anisotropy decay (A) and MEM analysis (B) of 1 $\mu$M HIV-1 protease in 100 mM NaOAc (pH 4.7), 1 M NaCl, at 37 °C. Excitation was set at 300 nm, and emission was collected at 348.8 nm.

Table 2: Parameters of MEM Anisotropy Decay Analysis

| substance | $B_1$ (%) | $\phi_1$ (ps) | $B_2$ (%) | $\phi_2$ (ns) | $\chi^2$ |
|---|---|---|---|---|---|
| apo | 19.2 | 250 | 80.7 | 12.96 | 1.26 |
| **1** | 16.9 | 276 | 75.8 | 11.95 | 1.40 |
| **2** | 12.9 | 354 | 81.3 | 11.82 | 1.89 |
| **3** | 15.2 | 265 | 84.7 | 10.97 | 1.60 |
| **4** | 11.7 | 308 | 88.2 | 11.04 | 1.63 |
| **5** | 17.0 | 293 | 81.9 | 11.86 | 1.49 |
| **6**[a] | 22.9 | 283 | 77.0 | 10.07 | 1.45 |
| **7** | 10.1 | 285 | 89.8 | 10.59 | 1.71 |
| **8** | 11.8 | 330 | 88.2 | 10.47 | 1.56 |
| **9** | 14.0 | 238 | 85.9 | 10.13 | 1.52 |
| **10** | 12.59 | 257 | 87.4 | 10.55 | 1.76 |
| **11**[b] | 14.2 | 325 | 26.7 | 5.11 | 1.39 |

[a] *Invirase* (Roche). [b] Analysis of the anisotropy decay of the penicillin derivative (**11**) yielded an additional limiting anisotropy, the amplitude of which is 58.9%.

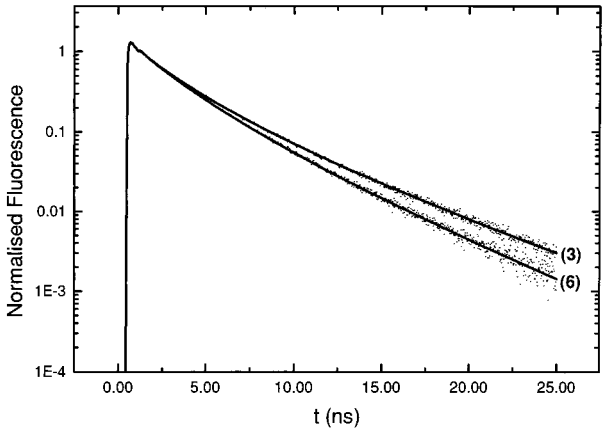


FIGURE 6: Time-resolved fluorescence decays of HIV-1 protease in complex with the benzimidazole−phosphatidylphenylstatine derivative (**3**) and with the isoquinoline hydroxyethylamine derivative (**6**). The experimental conditions were the same as described in Figure 4.

by MEM analysis are summarized in Table 1 and Table 2. The mean fluorescence lifetime $\tau_{mean}$ of nearly all complexes increased upon inhibitor binding as a result of a small increase of each lifetime component $\tau_i$. The reason for prolonged fluorescence lifetimes of the complexes is a change of the chromophores' local environments leading to a slower deactivation rate of the excited state. Commonly, reduced solvent exposure is associated with prolonged fluorescence lifetimes. The mean lifetime remains unchanged compared to the uncomplexed enzyme, only in complex with the isoquinoline-containing hydroxyethylamine derivative (**6**) due to the decrease of $\tau_4$ which compensates for the increases of $\tau_2$ and $\tau_3$ (see Figure 6). Besides representing a minor contribution to the protease decay, the short lifetime $\tau_1$ appears only when the protease is complexed with the morpholine-containing homostatine derivative (**9**). This means that in all other complexes this very specific quenching channel of the W42 residues has disappeared similar to the situation at longer emission wavelengths. Interestingly, introducing a phosphate group on the phenyl group (P3 site) of the benzimidazole-containing statine derivative (**1**) gave **3** which showed a significantly different fluorescence decay behavior. The appearance of three nanosecond lifetime distributions at 2.09, 3.69, and 5.49 ns is interpreted as being due to significant asymmetry introduced into the molecular complex by binding of **3**. The additional charged group leads to different decay times of one tryptophan species in the two protease subunits. Since the W42 side chains are much closer to the inhibitor binding site than the W6 residues, it is more likely that the W42 and W42′ side chains sense the asymmetry induced by binding of **3**, and therefore each decays with a characteristic nanosecond lifetime (3.69 and 5.49 ns, respectively).

Inhibitor binding was also shown to significantly influence the fluorescence anisotropy decay of the HIV-1 protease (see Table 2). The local motions of the tryptophan residues in the complexes, as expressed in the rotational correlation time $\phi_1$, became slower compared to those in the uncomplexed enzyme. The highest $\phi_1$ values were obtained for the molecular complexes with the *o*-hydroxy-*p*-methoxyphenyl-containing statine derivative (**2**), with the paracyclophane derivative (**8**), and with the symmetric penicillin derivative (**11**). The decreased mobility of the tryptophan residues in the inhibitor complexes of the HIV protease is in good agreement with the observed longer fluorescence lifetimes (see Table 1). Shielding the chromophores from solvent

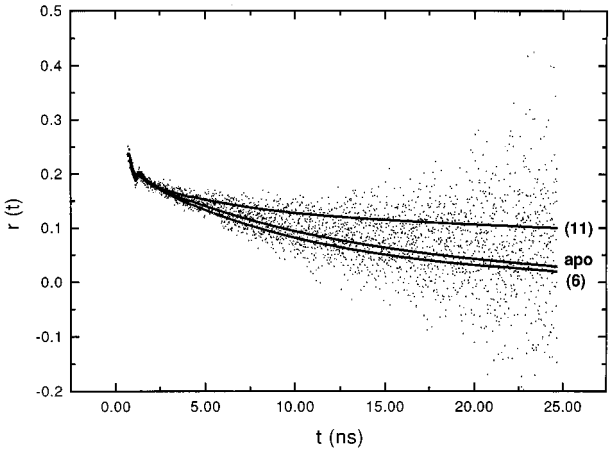


FIGURE 7: Time-resolved anisotropy decay of the HIV-1 protease compared with the decays of the molecular complexes with the isoquinoline hydroxyethylamine derivative (**6**) and with the penicillin derivative (**11**). The experimental conditions were the same as described in Figure 5.

(increased $\tau_{mean}$) means less mobility (increased $\phi_1$) due to more apolar contacts with surrounding hydrophobic residues.

The overall rotational correlation time $\phi_2$ of the HIV-1 protease decreased upon inhibitor binding (see Table 2 and Figure 7) as the result of inhibitor-induced flap closing, thereby reducing the hydrodynamic volume of the complexes. This is in accordance with published X-ray structures of protease inhibitor complexes (Figure 1). The most compact (smallest diameter) complex is obtained with the morpholine-containing derivative (**9**), whereas the most extended complex is formed with the benzimidazole-containing derivative (**1**). Another important readout of the protease inhibitor complex anisotropy measurements is the occurrence of a limiting anisotropy most pronouncedly in the decay of the symmetrical penicillin derivative (**11**) (see Figure 7). This limiting anisotropy is most probably the result of unspecific aggregation of the protease, as observed for the uncomplexed protein at 323 K. The different effects on the hydrodynamic volume, shrinking and aggregation, are illustrated in comparison to the uncomplexed HIV-1 protease in Figure 7.

## DISCUSSION

Characterizing drug receptor interactions should yield new insights into the mechanism by which inhibitors act, and therefore open new ways for developing better drugs (*1*). The HIV-1 protease in complex with many of its inhibitors is structurally and mechanistically one of the best characterized enzymes (*5*, *43*). However, besides knowing the three-dimensional structure of many HIV-1 protease inhibitor complexes, one essential aspect of these interactions has been underestimated, namely, the experimental determination of the dynamics of these complexes (*44*, *45*). Only recently the "importance of being floppy" (*46*) has been recognized for HIV-1 protease inhibitor complexes on the basis of NMR experiments (*47*). The authors showed that the side chains located in the substrate binding region as well as on the flap regions are less mobile than the rest of the molecule when an inhibitor is bound.

The time-resolved fluorescence experiments presented in this study showed that the tryptophan residues are excellent reporters for the molecular dynamics of HIV-1 protease inhibitor complexes. The demonstration of decreased side chain mobility as well as a reduction in the hydrodynamic molecular volume of the complexes, which has been revealed by the protease inhibitor complex anisotropy decays, is in good agreement with NMR and X-ray studies. With nano- to micromolar chromophore concentrations and approximately 15 min for a typical measurement, time-resolved fluorescence experiments are a sensitive and fast means for studying the molecular dynamics of protein ligand complexes.

In general, all 11 high-affinity inhibitors (see Figure 2) induced changes of the tryptophans' photophysics, including an increase of the mean fluorescence lifetime $\tau_{mean}$, an increase of the short rotational correlation time $\phi_1$, as well as a decrease of the long rotational correlation time $\phi_2$ (see Tables 1 and 2 and Figure 7). Structurally speaking, this means that binding of transition state analogues yields, relative to the uncomplexed protease, more compact molecular complexes with specific tryptophan surroundings and dynamics. In the time-resolved fluorescence intensity decays of the protease inhibitor complexes, the most inhibitor-dependent parameter is $\tau_4$ (see Table 1). From the emission wavelength dependence of the amplitudes $A_i$, we suggested that $\tau_4$ (together with $\tau_1$) is the intrinsic lifetime of the W42 chromophores. Since these side chains are located on the flap regions of the protease (Figure 1), they take part in the conformational rearrangements of the enzyme upon inhibitor binding. Therefore, chemically different inhibitors can give rise to different fluorescence decay constants of the W42 fluorophores.

We assume that the local chemical surrounding provided by the local secondary and tertiary structure is responsible for the value of $\tau_4$. Consequently, changes in the local environment induced by inhibitor binding are reflected in different $\tau_4$ values. The lifetime center $\tau_4$ of most protease inhibitor complexes is higher compared to the uncomplexed enzyme (see Table 1). This means that the W42 chromophores in the inhibitor complexes experience less collisions with solvent and/or are exposed to more hydrophobic contacts than in the unliganded protein. In complex with the phosphorylated benzimidazole-containing statine derivative (**3**), a very long fluorescence decay constant $\tau_4 = 5.49$ ns was observed. In addition, a fluorescence lifetime distribution at 3.69 ns was detected, which could not be found for any other protease inhibitor complex nor for the uncomplexed enzyme (see Table 1). These two fluorescence lifetimes are interpreted as arising from the two W42 chromophores, each decaying differently in complex with **3**. The additional phosphate group on the phenyl ring at the P3 site of **3** obviously introduced a significant asymmetry compared to **1** in the binding site, which has a major impact on the individual W42 fluorescence decays.

The symmetrical penicillin derivative **11** also gave a rather large value for $\tau_4 = 5.02$ ns, but no additional nanosecond lifetime component was detected like for the **3** complex. Moreover, a limiting anisotropy was found for this complex (see Figure 7) which is interpreted as being most likely the result of aggregation of the complexed molecules. In complex with **11**, there are more hydrophobic contacts with the W42 chromophores, which is characteristic for (unspecific) molecular aggregates, and which is reflected in the rather long lifetime $\tau_4$ of this complex.

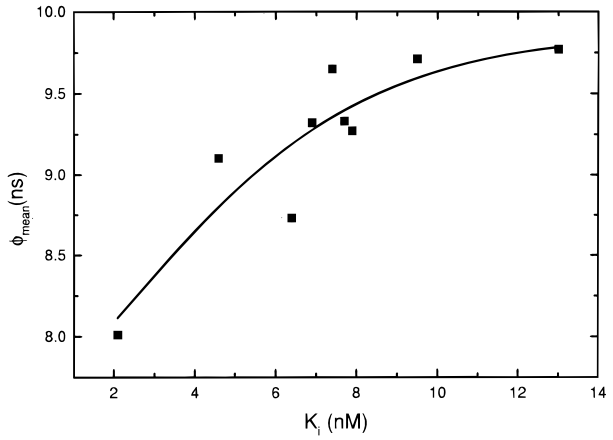


FIGURE 8: Correlation of the mean rotational correlation time $\phi_{mean}$ with the dissociation constants $K_i$ of the HIV-1 protease inhibitors. The data points were fitted according to a hyperbolic curve.

There is only one protease inhibitor complex for which a shorter $\tau_4$ value has been found than in the unliganded enzyme (Table 1). Obviously the W42 environment within the flaps of the HIV-1 protease in complex with the isoquinoline-containing hydroxyethylamine derivative **6** is different compared to the other complexes in such a way that more frequent solvent collisions can lead to the observed shorter intrinsic lifetime of the W42 residues. We hypothesize that this environment of the W42 residues, which is also but less pronouncedly observed in the **5** complex, is a characteristic structural feature which leads to the good inhibitory activity data of these two compounds.

From the time-resolved fluorescence anisotropy experiments, we have observed that binding of inhibitors to the HIV-1 protease resulted in a decreased mobility of the tryptophan side chains, as expressed by the increased $\phi_1$ values. This was accompanied by a reduction in the hydrodynamic volume, as shown by the decreased overall rotational correlation times $\phi_2$. Mechanistically, specific binding of an inhibitor (or ligand) to its receptor involves electrostatic and hydrophobic interactions with certain side chains in the binding site. The magnitude of these interactions depends on the chemical nature of the inhibitor and is therefore the reason not only for a certain $K_i$ value but also for inhibitor-specific structural rearrangements of the receptor protein. Different pharmacophoric interaction patterns between inhibitor (ligand) and HIV-1 protease (receptor) lead, besides specific interaction patterns in the substrate binding site, to specific conformational changes of the entire protein. This structural change is reflected in the rotational correlation times of the protease obtained from time-resolved anisotropy measurements. Since both inhibitor-specific side chain motions as well as the overall rotation are a measure of the structural rearrangements induced by an inhibitor, a correlation of the $K_i$ values with time-resolved fluorescence anisotropy parameters seemed possible. Our experiments have shown that, although no single rotational correlation time correlates with the $K_i$ values, the "composed" parameter $\phi_{mean}$ does so referring to inhibitor-specific contributions of the side chain dynamics relative to the overall rotation of the complexes. By definition, $\phi_{mean}$ [$=b_1\phi_1 + b_2\phi_2$ ($b_i = B_i/100$)] is the average anisotropy decay constant consisting of the relative (amplitude-weighted) contributions of the depolarizing modes ($\phi_1$ and $\phi_2$). Therefore, the value of $\phi_{mean}$ represents a measure of the global dynamics of the molecular complexes. A hyperbolic correlation of $\phi_{mean}$ with the inhibitor dissociation (inhibition) constant $K_i$ was revealed (see Figure 8). Only $\phi_{mean}$ correlates with the $K_i$. No single value, amplitude or rotational correlation time, exhibits this correlation. Consequently, a low global dynamic parameter $\phi_{mean}$ represents a new and easily accessible parameter for the optimization of activity of HIV-1 protease inhibitors.

## ACKNOWLEDGMENT

The inhibitors were provided by P. Ettmayer, P. Lehr, E. Schreiner, and D. Scholz, who are hereby gratefully acknowledged. We thank H. Radziner-Vyplel for his assistance in preparing the molecular graphics of the HIV-1 protease, as well as P. J. Andrew for critically reading the manuscript.

## REFERENCES

1. De Clercq, E. (1995) *J. Med. Chem. 38*, 2491−2517.
2. Mitsuya, H., Yarchoan, R., and Broder, S. (1990) *Science 249*, 1533−1544.
3. Gait, M. J., and Karn, J. (1995) *Trends Biotechnol. 13*, 430−438.
4. Collier, A. C., Coombs, R. W., Schoenfeld, D. A., Bassett, R. L., Timpone, J., Baruch, A., Jones, M., Facey, K., Whitacre, C., McAuliffe, V. J., Friedman, H. M., Merigan, T. C., Reichman, R. C., Hooper, C., and Corey, L. (1996) *N. Engl. J. Med. 334*, 1011−1017.
5. Wlodawer, A., and Erickson, J. W. (1993) *Annu. Rev. Biochem. 62*, 543−585.
6. Wlodawer, A., Miller, M., Jaskolski, M., Sathyanarayana, B. K., Baldwin, E., Wever, I. T., Selk, L. M., Clawson, L., Schneider, J., and Kent, S. B. H. (1989) *Science 245*, 616−621.
7. Appelt, K. (1993) *Perspect. Drug Discovery Des. 1*, 23−48.
8. Ringe, D. (1994) *Methods Enzymol. 241*, 157−177.
9. Gustchina, A., and Weber, I. T. (1990) *FEBS Lett. 269*, 269−272.
10. Umezawa, H., Aoyagi, T., Morishima, H., Matsuzaki, M., Hamada, M., and Takeuchi, T. (1970) *J. Antibiot. 23*, 259−262.
11. Debouck, C. (1992) *Res. Hum. Retroviruses 8*, 153−164.
12. Billich, A., Charpiot, B., Fricker, G., Gstach, H., Lehr, P., Peichl, P., Scholz, D., and Rosenwirth, B. (1994) *Antiviral Res. 25*, 215−233.
13. Miller, M., Schneider, J., Sathyanarayana, B. K., Toth, M. V., Marshall, G. R., Clawson, L., Selk, L., Kent, S. H. B., and Wlodawer, A. (1989) *Science 246*, 1149−1152.
14. Wonacott, A., Cooke, R., Hayes, F. R., Hann, M. M., Jhoti, H., McMeekin, P., Mistry, A., Murray-Rost, P., Singh, O. M., and Weir, M. P. (1993) *J. Med. Chem. 36*, 3113−3119.
15. Lam, P. Y. S., Jadhav, P. K., Eyermann, C. J., Hodge, C. N., Ru, Y., Bacheler, L. T., Meek, J. L., Otto, M. J., Rayner, M. M., Wong, Y. N., Chang, C.-H., Weber, P. C., Jackson, D. A., Sharpe, T. R., and Erickson-Viitanen, S. (1994) *Science 263*, 380−384.
16. Pearlman, D. A., and Murcko, M. A. (1996) *J. Med. Chem. 39*, 1651−1663.
17. Eftink, M. R. (1991) *Methods Biochem. Anal. 35*, 127−205.
18. Lakowicz, J. R. (1983) *Principles of Fluorescence Spectroscopy*, Plenum Press, New York/London.
19. Steiner, R. F. (1991) in *Topics in Fluorescence Spectroscopy 2* (Lakowicz, J. R., Ed.) Plenum Press, New York/London.
20. Elofsson, A., Nilsson, L., and Rigler, R. (1990) *Int. J. Pept. Protein Res. 36*, 267−301.
21. Axelsen, P. H., Gratton, E., and Prendergast, F. G. (1991) *Biochemistry 30*, 1173−1179.
22. Jones, B. E., Beechem, J. M., and Matthews, C. R. (1995) *Biochemistry 34*, 1867−1877.
23. Seelmeier, S., Schmidt, H., Turk, V., and von der Helm, K. (1988) *Proc. Natl. Acad. Sci. U.S.A. 85*, 6612−6616.

24. Billich, A., Hammerschmid, F., and Winkler, G. (1990) *Biol. Chem. Hoppe-Seyler 371*, 265−272.
25. Richards, A., Phylip, L. H., Farmerie, W. G., Scarborough, P. E., Alvarez, A., Dunn, B. M., Hirel, P. H., Konvalinka, J., Strop, P., Pavlickova, L., Kostka, V., and Kay, J. (1990) *J. Biol. Chem. 265*, 7733−7736.
26. Scholz, D., Billich, A., Charpiot, B., Ettmayer, P., Lehr, P., Rosenwirth, B., Schreiner, E., and Gstach, H. (1994) *J. Med. Chem. 37*, 3079−3089.
27. Billich, A., Fricker, G., Müller, I., Donatsch, P., Ettmayer, P., Gstach, H., Lehr, P., Peichl, P., Scholz, D., and Rosenwirth, B. (1995) *Antimicrob. Agents Chemother. 39*, 1406−1413.
28. Lehr, P., Billich, A., Charpiot, B., Ettmayer, P., Scholz, D., Rosenwirth, B., and Gstach, H. (1996) *J. Med. Chem. 39*, 2060−2067.
29. Ettmayer, P., Billich, A., Hecht, P., Rosenwirth, B., and Gstach, H. (1996) *J. Med. Chem. 39*, 3291−3299.
30. Roberts, N. A., Martin, J. A., Kinchington, D., Broadhurst, A. V., Craig, J. C., Duncan, I. B., Galpin, S. A., Handa, B. K., Kay, J., Kröhn, A., Lambert, R. W., Merrett, J. H., Mills, J. S., Parkes, K. E. B., Redshaw, S., Ritchie, A. J., Taylor, D. L., Thomas, G. J., and Machin, P. J. (1990) *Science 248*, 358−361.
31. Thompson, W. J., Fitzgerald, P. M. D., Holloway, M. K., Emini, E. A., Darke, P. L., McKeever, B. M., Schleif, W. A., Quintero, J. C., Zugay, J. A., Tucker, T. J., Schwering, J. E., Homnick, C. F., Nunberg, J., Springer, J. P., and Huff, J. R. (1992) *J. Med. Chem. 35*, 1685−1701.
32. Holmes, D. S., Clemens, I. R., Cobley, K. N., Humber, D. C., Kitchin, J., Orr, D. C., Patel, B., Paternoster, I. L., and Storer, R. (1993) *Bioorg. Med. Chem. Lett. 3*, 503−508.
33. O'Connor, D. V., and Phillips, D. (1984) *Time-Correlated Single Photon Counting*, Academic Press, London.
34. van Hoek, A., Vos, K., and Visser, A. J. W. G. (1987) *IEEE J. Quantum Electron. QE−23*, 1812−1820.
35. Visser, A. J. W. G., van Engelen, J., Visser, N. V., van Hoek, A., Hilhorst, R., and Freedman, R. B. (1994a) *Biochim. Biophys. Acta 1204*, 225−234.
36. Visser, N. V., Visser, A. J. W. G., Konc, T., Kroh, P., and van Hoek, A. (1994b) *Proc. SPIE 2137*, 618−626.
37. Livesey, A. K., and Brochon, J.-C. (1987) *Biophys. J. 52*, 693−706.
38. Bastiens, P. I. H., van Hoek, A., Benen, J. A. E., Brochon, J.-C., and Visser, A. J. W. G. (1992) *Biophys. J. 63*, 839−853.
39. Eftink, M. R., and Ghiron, C. A. (1976) *Biochemistry 15*, 672−680.
40. Chen, L. X.-Q., Engh, R. A., and Fleming, G. R. (1988) *J. Phys. Chem. 92*, 4811−4816.
41. Rayner, D. M., and Szabo, A. G. (1978) *Can. J. Chem. 56*, 743−745.
42. Ross, J. A., Schmidt, C. J., and Brand, L. (1981) *Biochemistry 20*, 4369−4377.
43. West, M. L., and Fairlie, D. P. (1995) *Trends Pharmacol. Sci. 16*, 67−74.
44. Royer, C. A., Tauc, P., Herve, G., and Brochon, J.-C. (1987) *Biochemistry 26*, 6472−6478.
45. Harrison, R. W., and Weber, I. T. (1994) *Protein Eng. 7*, 1353−1363.
46. Wagner, G. (1996) *Nat. Struct. Biol. 2*, 255−257.
47. Nicholson, L. K., Yamazaki, T., Torchia, D. A., Grzesiek, S., Bax, A., Stahl, S. J., Kaufman, J. D., Wingfield, P. T., Lam, P. Y. S., Jadhav, P. K., Hodge, C. N., Domaille, P. J., and Chang, C.-H. (1995) *Nat. Struct. Biol. 2*, 274−280.
48. Scholz, D., Billich, A., Charpiot, B., Ettmayer, P., Lehr, P., Rosenwirth, B., Schreiner, E., and Gstach, H. (1994) *J. Med. Chem. 37*, 3079−3089.

BI971654W